Exploring STEAP1 Expression in Prostate Cancer Cells in Response to Androgen Deprivation and in Small Extracellular Vesicles

Candice L. Bizzaro[1,2,3], Camila A. Bach[1,2,4,5], Ricardo A. Santos[1,2], Cecilia E. Verrillo[1,2], Nicole M. Naranjo[1,2], Ishan Chaudhari[1,2], Francis J. Picone[2], Waleed Iqbal[6], Ada G. Blidner[4], Gabriel A. Rabinovich[4,5], Alessandro Fatatis[6,7], Justine Jacobi[8], David W. Goodrich[8], Kevin K. Zarrabi[9], Wm. Kevin Kelly[9], Matthew J. Schiewer[2,3], and Lucia R. Languino[1,2]

Downloaded from http://aacrjournals.org/mcr/article-pdf/doi/10.1158/1541-7786.MCR-24-0903/3597404/mcr-24-0903.pdf by Drexel University user on 19 May 2025

ABSTRACT

The six-transmembrane epithelial antigen of the prostate (STEAP; STEAP1 and STEAP2) metalloreductases are therapeutic targets for advanced prostate cancer, and their expression has been linked to androgen receptor (AR) signaling; however, the regulatory mechanism and functions of STEAP1 and STEAP2 in prostate cancer progression remain elusive. In this study, we explore how *in vitro* androgen modulation and AR inhibition influence the expression of STEAP family members in cell lines with varying reliance on androgen signaling. Our data show that in response to androgen deprivation, *STEAP1* and *STEAP2* exhibit elevated transcript levels, whereas *STEAP4* levels are reduced, mirroring the expression profile of kallikrein-related peptidase 3 (*KLK3*). As STEAP1 and STEAP2 are implicated in the exocytic pathway, we evaluated expression profiles in small extracellular vesicles (sEV) released from prostate cancer cells and in circulating sEVs. STEAP1, but not STEAP2, is upregulated in sEVs from AR-negative cells, which express low cellular STEAP1, and AR-positive cells, which express high cellular STEAP1. These results indicate selective packaging of STEAP1 in prostate cancer cell–derived sEVs, irrespective of AR status and cellular STEAP1 expression levels. Finally, *ex vivo* analysis of circulating sEVs from genetically engineered mice carrying prostate cancer shows that STEAP1 is found in the sEV cargo and that its levels are independent of protumorigenic β1 integrin expression in the prostatic epithelium.

Implications: Understanding how androgen dependence affects STEAP1 expression in both tumor cells and sEVs across distinct disease stages will illuminate the clinical benefit of combinatorial AR and STEAP1-directed therapies and inform the optimal placement of STEAP1 targeting within the prostate cancer disease continuum.

Introduction

Prostate cancer

Prostate cancer is a multifaceted disease, with approximately 300,000 new cases diagnosed annually in the United States (1). The standard of care for locally advanced and metastatic disease is a combination of androgen deprivation therapy (ADT) and direct receptor antagonists, such as enzalutamide. However, castrate resistance is an inevitable reality for nearly all patients, hallmarked by a resurgence of androgen receptor (AR) activity (2). The selective pressure of androgen blockade drives adaptive resistance mechanisms via extensive transcriptomic reprogramming, resulting in disease progression often in incurable stages, including castrate-resistant prostate cancer (CRPC) and neuroendocrine prostate cancer (NEPC; refs. 3, 4). Primary prostate cancer has a low mutational burden; however, late-stage disease presents with various AR aberrations, including the emergence of constitutively active splice variant (ARV7) or complete loss of AR signaling, rendering AR-directed therapies ineffective (3–6). Moreover, the transition to advanced disease stages is transcriptionally heterogeneous, resulting in distinct molecular subtypes and significant inter-patient variability (5, 6). This presents a significant clinical challenge and highlights the need to develop novel diagnostic methods and therapeutics.

STEAP family proteins in prostate cancer

The six-transmembrane epithelial antigen of the prostate (STEAP) is a family of cell surface metalloreductases comprised of four members: STEAP1, STEAP2, STEAP3, and STEAP4. In mammals, STEAP1–4 regulate intracellular stress, inflammation, and proliferation by mediating iron and copper homeostasis (7). Although all STEAP family members share similar structural homology and localization patterns, each protein retains distinct cellular functions (8). Elevated expression of STEAP 1, 2, and 4 has been implicated in tumorigenesis contributing to prosurvival and migratory phenotypes and correlates with poor survival outcomes (7, 9–13). Previous

[1]Prostate Cancer Discovery and Development Program, Thomas Jefferson University, Philadelphia, Pennsylvania. [2]Department of Pharmacology, Physiology, and Cancer Biology, Thomas Jefferson University, Philadelphia, Pennsylvania. [3]Department of Urology, Thomas Jefferson University, Philadelphia, Pennsylvania. [4]Laboratory of Glycomedicine, Institute of Biology and Experimental Medicine, National Council of Scientific and Technical Investigations, Buenos Aires, Argentina. [5]Faculty of Exact and Natural Sciences, University of Buenos Aires, Argentina. [6]Department of Pharmacology and Physiology, Drexel University College of Medicine, Philadelphia, Pennsylvania. [7]Sidney Kimmel Comprehensive Cancer Center, Thomas Jefferson University, Philadelphia, Pennsylvania. [8]Department of Pharmacology and Therapeutics, Roswell Park Comprehensive Cancer Center, Buffalo, New York. [9]Department of Medical Oncology, Thomas Jefferson University, Philadelphia, Pennsylvania.

C.L. Bizzaro and C.A. Bach contributed equally to this article.

Corresponding Author: Lucia R. Languino, Bluemle Life Sciences, Building 233 South 10th Street, Suite 506, Philadelphia, PA 19107. E-mail: lucia.languino@jefferson.edu

Mol Cancer Res 2025;XX:XX–XX

doi: 10.1158/1541-7786.MCR-24-0903

©2025 American Association for Cancer Research

studies reported that blocking STEAP1 with an mAb reduces *in vitro* cellular communication between cancer cells and *in vivo* tumor progression, establishing a role of STEAP1 as a mediator of intercellular communication in prostate cancer pathogenesis (14–16). Downregulation of STEAP1 alters the expression of 110 proteins linked to extracellular vesicles (EV; ref. 11). This suggests that extracellular STEAP1 interacts with the tumor microenvironment contributing to cell growth, invasion, and metastasis (11, 14–16). Although STEAP1 involvement in prostate cancer pathogenesis is apparent, the precise regulatory mechanisms and contributions to cancer progression remain unclear.

It is well established that STEAP proteins are regulated by the AR signaling network (7). STEAP1 tissue-restricted expression, enrichment in malignant tissue, and cell surface localization make it an attractive therapeutic target for primary and metastatic prostate cancer (7). IHC analysis of organ-confined and metastatic CRPC (mCRPC) indicated that STEAP1 exhibits greater intratumoral homogeneity and consistency across distinct metastatic sites than prostate-specific membrane antigen (PSMA), another therapeutic target (5). Single-cell analysis from patients with late-stage CRPC and NEPC revealed a tight correlation among STEAP1, STEAP2, and AR-positive gene regulatory networks, highlighting broader expression than PSMA across transcriptomically distinct molecular subtypes (6). Furthermore, STEAP1 and STEAP2 have demonstrated promising clinical utility as a tumor antigen for T cell–redirecting therapies, including the bispecific T-cell engagers (i.e., xaluritamig; AMG 509) or CAR T-cell therapy, in clinical and preclinical investigations (5, 17–19). This highlights the potential of STEAP1 and STEAP2 as biomarkers and therapeutic targets in prostate cancer.

EVs in prostate cancer

EVs are membrane-enclosed structures released from cells that play a crucial role in cell-to-cell communication and influence cell motility contributing to cancer progression (20–23). sEVs, ranging from 100 to 200 nm, are often of endosomal origin and carry a diverse array of cargo. Their abundance in serum, plasma, urine, and saliva makes them a potential modality for noninvasive disease monitoring (20, 21). Prior research studies have shown that sEVs derived from prostate cancer cells influence differentiation, angiogenesis, metastasis, anchorage-independent growth, and premetastatic niche formation by transferring protumorigenic cargoes to distant cells (24–28). However, studies have yet to assess the systemic, long-term impacts of prostate cancer–derived sEVs on the tumor microenvironment and the protein pathway involved in this process.

Here, we show androgen deprivation context–dependent effects on the expression of *STEAP1* and *STEAP2* compared with *STEAP4*. Moreover, the deviations in *STEAP1* regulation correlate with ARV7 status. Furthermore, we show that STEAP1 is found in sEVs isolated from human prostate cancer cells, whereas STEAP2 is minimally expressed, and we reveal the expression of STEAP1 in sEVs from prostate cancer–bearing mouse plasma.

Materials and Methods

Cell culture conditions

Human prostate cancer cells LNCaP (CRL-1740, RRID: CVCL_1379), C4-2 (CRL-3314, RRID: CVCL_4782), C4-2B (CRL-3315, RRID: CVCL_4784), DU145 (HTB-81, RRID: CVCL_0105), 22Rv1 (CRL_2505, RRID:CVCL_4735), and PC3 (CRL-3471, RRID: CVCL_B0E3) were obtained from ATCC and cultured as previously described (2, 29, 30). Cells were cultured for a period of approximately 2 months and then replaced by new thaws.

For pharmacologic AR manipulation assays, cells were seeded at equal densities, viability was ensured to be >70-80%, and harvested at 75% to 80% confluency. Cells were cultured in phenol red–free Improved Minimum Essential Medium (IMEM; Gibco, 10-026-CV) with 10% charcoal dextran–stripped FBS (HyClone, SH30086.03), 1% L-glutamine, and 1% penicillin–streptomycin (Gibco, 15140-122) for 72 hours before additional treatments with either enzalutamide (Selleck Chemicals, S1250) or 5α-DHT (Selleck Chemicals, S4757) at indicated doses and time points. All treatments were performed in triplicates. Control groups were treated with a concentration of DMSO (Invitrogen, D12345) equivalent to that of the highest dose.

Mouse models

Supplementary Table S1 describes the genotype of male mice used in this study. Animal care complied with standards established by the Office of Laboratory Animal Welfare, Department of Health and Human Services at NIH. Experimental protocols were approved by the Institutional Animal Care and Use Committee at Thomas Jefferson University.

Gene expression analysis

RNA was isolated using TRIzol (Invitrogen, 15596018) according to the manufacturer's protocol. RNA was quantified using NanoDrop OneC (Thermo Fisher Scientific), and the purity threshold was set at 2.0 for 260/280 nm ratio and 2.0–2.2 for 260/230 nm ratio. Pellets were stored at −80°C.

cDNA was generated using SuperScript IV VILO Master Mix (Invitrogen, 11755500) per the manufacturer's protocols. qPCR was conducted with the primers described in Supplementary Table S2 with QuantStudio 3 RT-PCR (Applied Biosystems, A28131) and Power SYBR Green PCR Master Mix (Applied Biosystems, 4367659) using 100 ng cDNA per well in technical triplicate. Genes were normalized to housekeeping gene *RPLPO* encoding 60S ribosomal subunit. Experiments were performed in $n = 3$ or $n = 4$ for each gene condition.

EV isolation from C4-2B, DU145, and PC3 cells by differential ultracentrifugation

EVs from cell culture supernatants of prostate cancer cells were isolated as previously described (25, 31, 32).

EV isolation from mouse plasma and sEV isolation by density gradient

For each EV preparation from mouse plasma, blood samples from mice with the same genotype ($n = 3$) and comparable age, collected by intracardiac puncture, were combined (25). Four preparations for each genotype were used. To obtain plasma, the isolated blood from mice was centrifuged at 16,100 × *g* for 30 minutes at 4°C. Afterward, EVs were precipitated using a polymer solution mixed with mouse plasma in a 1:4.16 ratio, incubated for 45 minutes at 4°C, and then spun down at 1,500 × *g* for 30 minutes at 4°C. The supernatant was removed, and the resulting EV precipitate was spun at 1,500 × *g* for 5 minutes at 4°C. The EVs were resuspended in 60 μL of PBS and were further isolated using iodixanol density gradient (IDG) separation, as described before (24). The 10 sEV fractions obtained were washed with 1 mL of PBS twice by centrifuging at 120,000 × *g* for 70 minutes at 4°C. The collected fractions were pooled and resuspended in 60 μL of

Downloaded from http://aacrjournals.org/mcr/article-pdf/doi/10.1158/1541-7786.MCR-24-0903/3597404/mcr-24-0903.pdf by Drexel University user on 19 May 2025

PBS as follows: low-density sEVs (ld-sEV, 1.101–1.136 g/mL), middle-density sEVs (md-sEV, 1.141–1.181 g/mL), and high-density sEVs (hd-sEV, 1.186–1.188 g/mL). The isolated sEV samples were stored at −80°C.

Nanoparticle tracking analysis

As previously published, nanoparticle tracking analysis (NTA; RRID: SCR_014239) was used to determine the size distribution and concentration of sEVs derived from prostate cancer cells and from β1 FF, and β1 FF TRAMP (TR) mouse plasma (24, 31).

ZetaView NTA

NTA was performed using the ZetaView QUATT (Particle Metrix, RRID: SCR_016647) to assess the size distribution and concentration of sEVs derived from β1 FF, β1 FF TR, wild-type, and TR mouse plasma. A 1.5 mL aliquot of diluted sEVs was loaded into the instrument. For each measurement, 11 positions were scanned, and 60 frames per position were captured (video settings: high) using the 488-nm laser with the following instrument parameters: scatter filter wavelength, sensitivity at 80, shutter at 100, minimum brightness at 20, and cell temperature at 23°C.

Lysate preparation

Cells were lysed with RIPA buffer [RIPA buffer composition: 150 mmol/L NaCl (Fisher Chemical, S271-10), 1.0% NP-40 (Fisher Chemical, 85124), 0.5% deoxycholate (Alfa Aesar, J62288), 0.1% SDS (Invitrogen, AM9823), and 50 mmol/L Tris pH 8.0 (Fisher Chemical, BP152-5) along with an inhibitor cocktail containing 50 μL of 1 mol/L NaF (Fisher Chemical, S299), 10 μL Halt Protease Inhibitor (Thermo Fisher Scientific, 1862209), 10 μL phenylmethylsulfonylfluoride (Acros Organics, 329-96-6), and 0.013 g β-glycerophosphate (Acros Organics, 13408-09-8). Total protein quantification was performed by DC Protein Assay Kit (Bio-Rad, 5000111) according to the manufacturer's protocol.

Immunoblotting

The immunoblotting (IB) analysis of C4-2B, DU145, and PC3 total cell lysates and their derived sEVs and sEVs from mouse plasma was conducted as previously described (24, 31, 33). For LNCaP and C4-2, IB was performed using 10% Bio-Rad gels (Bio-Rad, 546-1033).

All primary antibodies were handled as per the manufacturer's protocol. Rabbit mAbs to STEAP1 (Cell Signaling Technology, 88677, RRID: AB_2800128, 1:1,000), β-Actin (Cell Signaling Technology, 4970, RRID: AB_2223172, 1:1000), and TSG101 (Abcam, ab125011, RRID: AB_10974262, 1:1,000) were used. Rabbit polyclonal antibodies to calnexin (CNX; Abcam, ab22595, RRID: AB_2069006, 1:1,000), c-Src (Santa Cruz Biotechnology, sc-18, RRID: AB_631324, 1:250), STEAP2 (Proteintech, 2021-1-AP, RRID: AB_10665556, 1:500), STEAP4 (Proteintech, 11944-1-AP, RRID: AB_308517, 1:1,000), and AR (EMD Millipore, 06-680, RRID: AB_310214, 1:1,000) were used. Mouse mAbs to CD9 (Santa Cruz Biotechnology, SC-13118, RRID: AB_627213, 1:200), Alix (Bio-Rad, MCA2493, RRID: AB_872031, 1:250), CD81 (Abcam, ab23505, RRID: AB_447487, 1:1,000), and vinculin (Sigma-Aldrich, V9264, RRID: AB_10603627, 1:1,000) were used.

Densitometry and data analysis

ImageJ software (NIH, RRID: SCR_003070) was used to determine the band intensity of STEAP1 and loading markers. The analysis was done by normalizing each sample's pixel intensity (AUC) to loading.

RNAi

Transfection solution was prepared using ON-TARGETplus Human STEAP1 (26872) SMARTpool (Horizon Discovery, L-003713-01-0005) and siRNA ON-TARGET control (Horizon Discovery, D-001810-10-20) with Opti-MEM (Gibco, 31985-070) and DharmaFECT 4 (Horizon Discovery, T-200-03) for a final concentration of 10 nmol/L per well (Supplementary Table S3). C4-2 cells were seeded at 2.0×10^5 cells per well in a poly-L-lysine–coated six-well plate for overnight transfection in Opti-MEM.

In silico expression correlations

cBioPortal patient-derived datasets were queried to visualize gene correlations among *STEAP1*, *AR*, *KLK2*, *KLK3*, *KLK15*, *NKX3-1*, and *TMPRSS2*. Prostate adenocarcinoma (The Cancer Genome Atlas, Firehose Legacy) and metastatic prostate adenocarcinoma (SU2C/PCF Dream Team) mRNA expression from capture *Z*-scores was quantified by RNA Seq V2 RSEM and fragments per kilo base per million mapped fragments (FPKM), respectively (34). Expression distribution was measured for diploid tumors for each gene, in which the *Z*-score threshold was restricted to ±2 for all queries (35–37).

We obtained RNA sequencing (RNA-seq) data for 210 mCRPC samples previously described (38). The AR activity score was measured by the expression levels of seven genes, excluding *STEAP1* and *STEAP2*, previously described in ref. 39. The *Z*-scores of *KLK2*, *KLK3*, *FKBP5*, *PLPP1*, *RAB3B*, *NKX3-1*, and *ACLS3* were determined for each gene across all samples, and then both *STEAP1* and *STEAP2* were compared with average *Z*-scores for the seven genes, as well as *KLK3* by itself.

We separated the tumor samples into high and low *KLK3* expression samples by *Z*-scoring the log-transformed transcript per million (TPM) values by [$\log_2$(TPM + 1)]. We defined the *KLK3*-high samples as *Z*-scores >0.75 ($n = 26$), *KLK3*-low samples as *Z*-scores < −0.75 ($n = 28$), and intermediate samples corresponding to *Z*-scores between −0.75 and 0.75. Next, we compared the log-transformed TPM expression of *STEAP1* and *STEAP2* in both groups. Within the "low *KLK3*" group, we selected high *STEAP2* $\log_2$(TPM + 1) >6 expressing patients and looked at the corresponding *STEAP1* values to compare expression levels between matched patients.

Statistical analysis

Statistical analysis for gene expression and IB quantification was performed using GraphPad Prism 9 (GraphPad Software, Inc., RRID: SCR_002798) as described in the figure legends. *P* values ≤0.05 were considered statistically significant. Relative mRNA expression is shown as individual replicates with error bars representing mean ± SEM. *P* values were calculated using two-way ANOVA or mixed-model ANOVA with a 95% confidence interval followed by the indicated *post hoc* test.

Data availability

The data analyzed in this study were obtained through controlled access from the European Genome Archive (EGA) with ascension numbers EGAD00001008991, EGAD00001008487, and EDAG00001009065.

Results

Alterations in the expression of STEAP family members in response to androgen deprivation

We investigated changes in the transcript levels of *STEAP1*, *STEAP2*, *STEAP4*, and *KLK3*, a classical AR target gene, in response to androgen deprivation. Hormone therapy–sensitive (HTS) LNCaP,

Downloaded from http://aacrjournals.org/mcr/article-pdf/doi/10.1158/1541-7786.MCR-24-0903/3597404/mcr-24-0903.pdf by Drexel University user on 19 May 2025

CRPC C4-2, and CRPC 22Rv1 cells were used to evaluate how varying reliance on androgen signaling affects STEAP expression profiles. Cells were cultured in charcoal-stripped serum (CSS) to model androgen deprivation *in vitro*. CSS removes exogenous hormones and precursors, reducing AR-dependent ligand activation, which is confirmed by an evident decrease in *KLK3* in LNCaP and 22Rv1 cells (**Fig. 1A**). For LNCaP and C4-2 cells, which rely on ligand-activated full-length AR, *STEAP1* and *STEAP2* transcripts increase under androgen deprivation conditions (**Fig. 1A**), whereas *STEAP4* transcript decreases mirroring the expression profile of *KLK3* or does not change (**Fig. 1A**). In contrast, 22Rv1 cells, expressing ARV7, a constitutively active AR variant that lacks the ligand-binding domain, show *STEAP1* and *STEAP2* decrease in response to androgen deprivation (**Fig. 1A**). As STEAP1 is a therapeutic target of interest, we validated these results at the protein level by IB, observing the same trend in expression (**Fig. 1B**). Total AR protein levels are slightly decreased, although results are nonsignificant as CSS reduces AR transcriptional output rather than affecting the protein level. To examine how combinatorial AR blockade affects STEAP expression, we treated cells with increasing doses of enzalutamide, a competitive AR inhibitor that blocks ligand binding and nuclear translocation (Supplementary Fig. S1). Across all cell lines, the transcriptional changes observed in response to androgen deprivation remain consistent, recapitulating the expression profiles in **Fig. 1A**. Under regular growth conditions, the effect of enzalutamide is negligible, and the combination does not significantly alter the response compared with androgen deprivation alone (Supplementary Fig. S1).

These data confirm that *STEAP1* and *STEAP2* transcripts are elevated under low-androgen conditions, exhibiting inverse expression profiles compared with *STEAP4* and *KLK3*.

Rescue of STEAP1 expression is time dependent

We validated the dependence of STEAP expression on androgen signaling by using DHT to induce AR transcriptional activity. In LNCaP cells, 24-hour stimulation with DHT yields minimal changes in *STEAP1* expression under full-hormone or CSS conditions, regardless of dose (**Fig. 2A**). *STEAP2* follows the same expression pattern as *STEAP1* (Supplementary Fig. S2). The robust response of *KLK3* confirms AR transcriptional activity (**Fig. 2**). *STEAP4* parallels *KLK3*, indicative of positive AR regulation (**Fig. 2**; Supplementary Fig. S2). C4-2 cells mirror the response of LNCaP cells under all conditions (Supplementary Fig. S2). In contrast, 22Rv1 cells are responsive to 0.1 nmol/L dose of DHT under low-androgen conditions, exhibiting a twofold increase in *STEAP1* expression relative to androgen deprivation alone (**Fig. 2B**).

We did not observe an effect on *STEAP1* transcript levels using 10 nmol/L DHT for LNCaP and 22Rv1 cells at the 24-hour time point (**Fig. 2A** and **B**); therefore, we examined if DHT induced time-dependent expressional changes in *STEAP1* transcript levels. We evaluated transcript levels at 8, 16, and 24 hours after stimulation with 1 nmol/L DHT (**Fig. 2C**). For LNCaP cells under regular growth conditions, a mild reduction in *STEAP1* transcript is observed at the 8- and 16-hour time points (**Fig. 2C**). In LNCaP cells in which *STEAP1* is elevated upon androgen deprivation, stimulation with 1 nmol/L DHT for 8 and 16 hours reduces *STEAP1* expression to levels comparable with the control (**Fig. 2C**). The opposite is observed in 22Rv1 cells, such that *STEAP1* decreases with androgen deprivation, with DHT restoring expression to baseline across all time points (**Fig. 2D**). These findings suggest a temporal dependence of *STEAP1* transcriptional response with respect to AR stimulation in both cell lines.

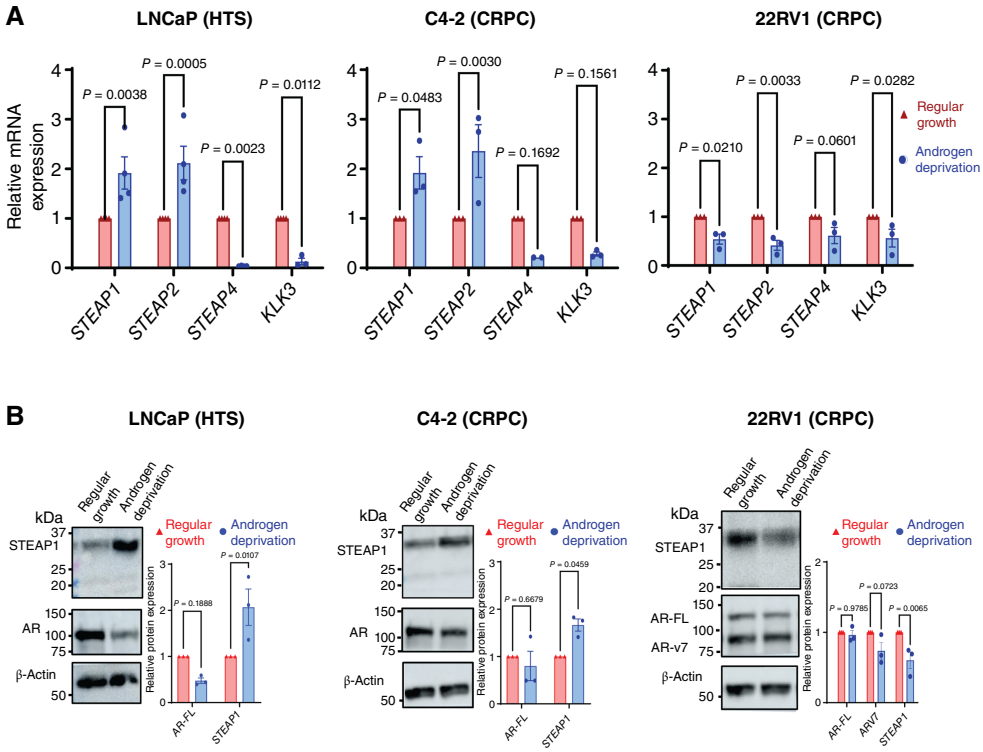


Figure 1.
Alterations in STEAP expression in response to androgen deprivation. **A,** Relative mRNA levels of *STEAP1*, *STEAP2*, *STEAP4*, and *KLK3* in LNCaP (left), C4-2 (middle), and 22Rv1 (right) cells 72 hours after plating under CSS conditions. **B,** Protein levels of STEAP1 and full-length AR (AR-FL) in LNCaP (left), C4-2 (middle), and AR-FL and ARV7 in 22Rv1 (right) cells 72 hours after plating in CSS. Cell lysates were loaded at 20 μg per well. Protein quantification (right) normalized to loading control β-Actin. *P* values were calculated by two-way ANOVA with multiple comparisons followed by the *post hoc* Šídák test.

Downloaded from http://aacrjournals.org/mcr/article-pdf/doi/10.1158/1541-7786.MCR-24-0903/3597404/mcr-24-0903.pdf by Drexel University user on 19 May 2025

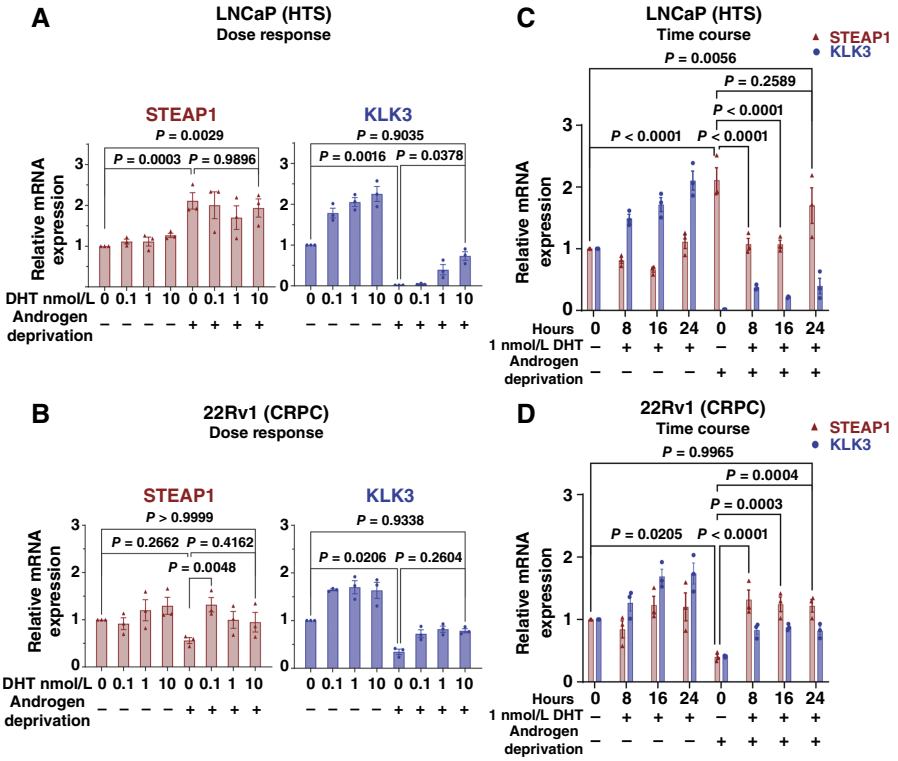


Figure 2.

Rescue of *STEAP1* mRNA expression is time dependent. **A** and **B,** Relative mRNA expression of *STEAP1* and *KLK3* in (**A**) LNCaP and (**B**) 22Rv1 cells treated with 0 nmol/L (DMSO) and 0.1, 1, and 10 nmol/L DHT for 24 hours under regular growth or CSS conditions. **C** and **D,** Relative mRNA expression of *STEAP1* and *KLK3* in (**C**) LNCaP and (**D**) 22Rv1 cells treated with either 0 nmol/L (DMSO) or 1 nmol/L DHT for 8-, 16-, and 24-hour time points under regular growth and CSS conditions. *P* values were calculated by two-way ANOVA with multiple comparisons followed by the *post hoc* Šídák test.

Expression analysis of STEAP1 and STEAP2 in patients with mCRPC

To examine clinical correlations between *STEAP1* and *AR*, we queried primary prostate adenocarcinoma (The Cancer Genome Atlas, Firehose Legacy) and metastatic prostate adenocarcinoma (SU2C/PCF Dream Team) cohorts from cBioPortal. We evaluated co-expression of *STEAP1* and *AR* mRNAs, as well as with canonical AR target genes (*KLK2*, *KLK3*, *KLK15*, *TMPRSS2*, and *NKX3-1*), as markers for AR activity. We observe a positive correlation in mRNA expression in primary adenocarcinoma, which becomes more pronounced in the metastatic cohort (Supplementary Fig. S3). To corroborate these results, we analyzed RNA-seq data from 210 mCRPC biopsies from patients who received prior ADT, as described in Quigley and colleagues (40). AR activity was defined as the average *Z*-score of seven AR target genes (*KLK2*, *KLK3*, *FKBP5*, *PLPP1*, *RAB3B*, *NKX3-1*, and *ACLS3*). A strong positive correlation between AR activity and *STEAP1* and *STEAP2* expression is observed (Supplementary Fig. S3). These data suggest a linear relationship between *STEAP1* transcript and AR activity with progression to advanced disease stages.

Within the 210-patient cohort, *KLK3* expression was evaluated as a surrogate marker for AR activity to classify patients based on clinical treatment response. The density distribution of $\log_2$-transformed TPM for *KLK3* captured expression variability across the cohort (**Fig. 3A**), whereas *Z*-scores allowed for comparison of each patient with the population mean (**Fig. 3B**). Patients were stratified into low, intermediate, and high *KLK3* expression groups. Low *KLK3* expression corresponds to low AR activity, indicating a clinical treatment response, whereas high *KLK3* corresponds to sustained AR activity, representing nonresponders (**Fig. 3A** and **B**). Approximately 75% of patients fall into the intermediate range with *Z*-scores between −0.75 and 0.75. The high-*KLK3* group concentrates around *Z*-scores between 0.75 and 1.5, indicating consistent AR activity among nonresponders. In contrast, the low-*KLK3* group shows greater variability (*Z*-scores between −4 and −0.75), reflecting heterogeneity in AR activity among responders (**Fig. 3B**).

Excluding the intermediate population, we examined *STEAP1* and *STEAP2* expression within the low *KLK3* (responder) and high *KLK3* (nonresponder) expression groups. Both *STEAP1* and *STEAP2* are enriched among nonresponders relative to responders, correlating with sustained AR activity (**Fig. 3C**). However, within the responder group, there is notably greater variability in expression $\log_2(\text{TPM} + 1)$ between 0 and 8, compared with the nonresponders, which concentrate around $\log_2(\text{TPM} + 1) > 8$ (**Fig. 3C**). A subset of patients in the low *KLK3* expression group (responders), highlighted with the green boxes, exhibits *STEAP1* and *STEAP2* expression levels more than two SDs above the population mean (**Fig. 3C**). This subset of patients show *STEAP1* and *STEAP2* expression comparable with the high-*KLK3* group (nonresponders). Furthermore, these responders show concordant expression, indicating that *STEAP1* and *STEAP2* are upregulated or downregulated in parallel (**Fig. 3D**). These findings show that despite low AR activity and reduced *KLK3*, some responders retain elevated *STEAP1* and *STEAP2* expression. Consequently, *KLK3* alone may not fully capture variability in therapeutic response, underscoring the complementary role of STEAP1 as a prognostic marker for different patient outcomes.

STEAP1 expression in human prostate cancer cells and derived sEVs

To investigate if STEAP1 is released and packed into sEVs, we evaluated its expression in sEVs derived from androgen-independent C4-2B, PC3, or DU145 human prostate cancer cells. sEVs were

Downloaded from http://aacrjournals.org/mcr/article-pdf/doi/10.1158/1541-7786.MCR-24-0903/3597404/mcr-24-0903.pdf by Drexel University user on 19 May 2025

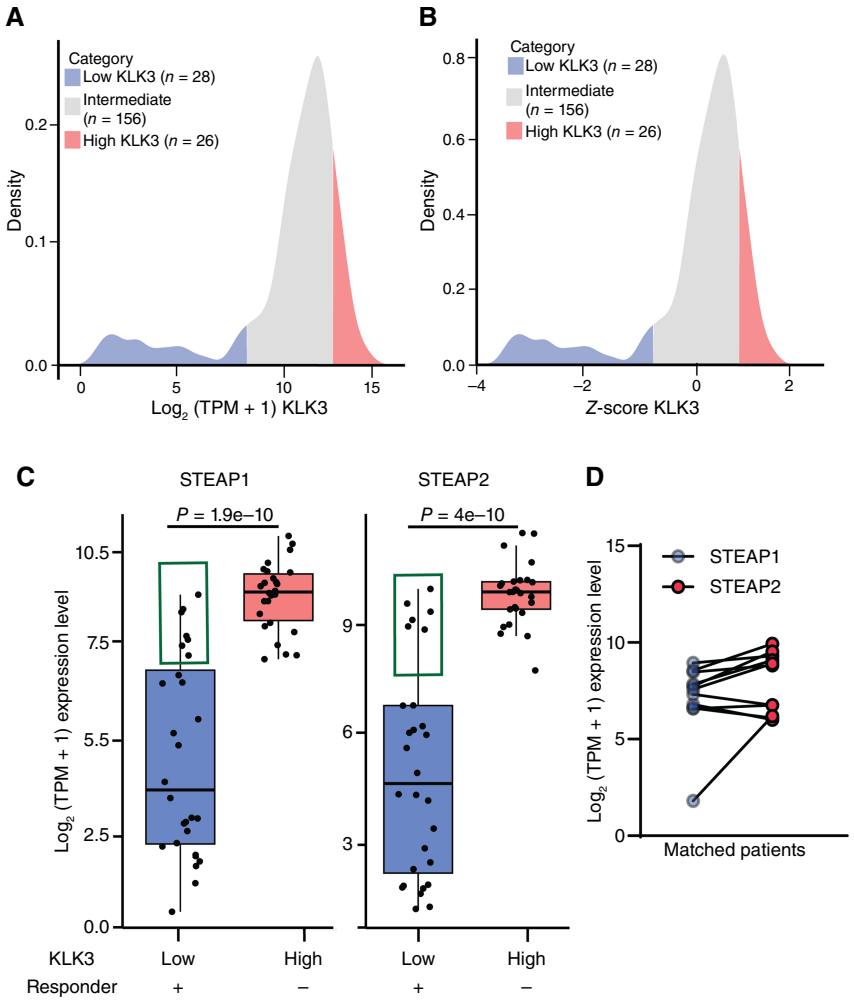


Figure 3.

Comparison of KLK3, *STEAP1*, and STEAP2 expression in clinical responders and nonresponders. **A,** Density plot of $\log_2$(TPM + 1) values corresponding to *Z*-scores (**B**) with cutoffs at $\log_2$(TPM + 1) < 8.023 and $\log_2$(TPM + 1) > 12.804 for low and high subgroups. **B,** Density plot of *KLK3* *Z*-scores with patients stratified into low (*Z*-score < −0.75), intermediate, and high (*Z*-score > 0.75) subgroups. **C,** Boxplots showing the expression levels of *STEAP1* (left) and *STEAP2* [right; $\log_2$(TPM + 1)] in patients classified as low *KLK3* (blue, responders) and high *KLK3* (red, nonresponders). where + refers to reponders and − refers to nonresponders. *P* values were determined by the Wilcoxon test. A subset of patients in the low *KLK3* expression group (responders), which exhibit *STEAP1* and *STEAP2* expression levels more than two SDs above the population mean, is highlighted with the green boxes. **D,** Expression of *STEAP1* and *STEAP2* [$\log_2$ (TPM + 1)] in individual patients from the low-*KLK3* and high-*KLK3* groups described in (**C**). Each line connects the *STEAP1* and *STEAP2* expression levels within a single patient.

isolated via ultracentrifugation followed by IDG separation. Classical sEV markers such as Alix, TSG101, or CD81 were used to characterize the C4-2B, PC3, and DU145 cell–derived sEVs (**Fig. 4A–D**). Additionally, the absence of CNX in the lysates from sEVs indicates that the analyzed sEV samples are free from contamination by the endoplasmic reticulum compartment (**Fig. 4C**).

To validate the specificity of the STEAP1 antibody, we downregulated the expression of STEAP1 in human C4-2 prostate cancer cells by transfecting them with a SMARTpool STEAP1 siRNA and showing that the STEAP1 antibody is specific (Supplementary Fig. S4). IB analysis of the individual IDG fractions of C4-2B sEVs reveals expression of STEAP1 in fractions 1 through 6 (**Fig. 4A**) and in DU145 sEVs (**Fig. 4B**). The sEV marker TSG101 is expressed in C4-2B and DU145 cells and their derived sEVs (**Fig. 4B** and **C**). Although STEAP1 is expressed in IDG fractions 3 and 5 of the sEVs derived from C4-2B and DU145 cells, STEAP2 is not expressed (**Fig. 4C**). Moreover, STEAP1 expression is increased in C4-2B and DU145 sEV fractions compared with their parental cells (**Fig. 4C**).

We combined IDG fractions based on their densities and analyzed those with densities between 1.141 and 1.181 g/mL as md-sEV–enriched fractions. STEAP1 is also detected in PC3 cells and their derived sEVs (**Fig. 4D**). Hence, STEAP1 is detectable across all prostate cancer cells tested and their derived sEVs, whereas STEAP2 is not. As expected, the tetraspanin CD81 is enriched in PC3-derived sEVs but is undetectable in PC3 total cell lysate (**Fig. 4D**). These findings are summarized in Supplementary Table S4. Moreover, NTA of sEVs derived from C4-2B, DU145, and PC3 cells shows that the size of these sEVs is between 150–250 nm (**Fig. 4E–G**). Therefore, our results show that C4-2B, DU145, or PC3-derived sEVs contain STEAP1.

STEAP1 expression in sEVs derived from plasma of mice carrying prostate cancer

As the expression of STEAP1 was confirmed in three prostate cancer cell lines and their derived sEVs, the next step was to assess whether circulating sEVs from mouse plasma contained STEAP1 (**Figs. 5** and **6**) and if STEAP1 expression in the prostatic epithelium is affected by the presence of β1 integrins, which are necessary for sEVs to support anchorage-independent growth (24). We used plasma from four genetically engineered mouse models: β1 FF mice, which have loxP sites flanking the *Itgb1* gene and produce nontumorigenic sEVs; β1 FF TR mice, whose sEVs exhibit enhanced tumorigenicity; and β1 FF Cre mice and β1 FF Cre TR mice, in which Cre recombinase enables localized deletion of the *Itgb1* gene

Downloaded from http://aacrjournals.org/mcr/article-pdf/doi/10.1158/1541-7786.MCR-24-0903/3597404/mcr-24-0903.pdf by Drexel University user on 19 May 2025

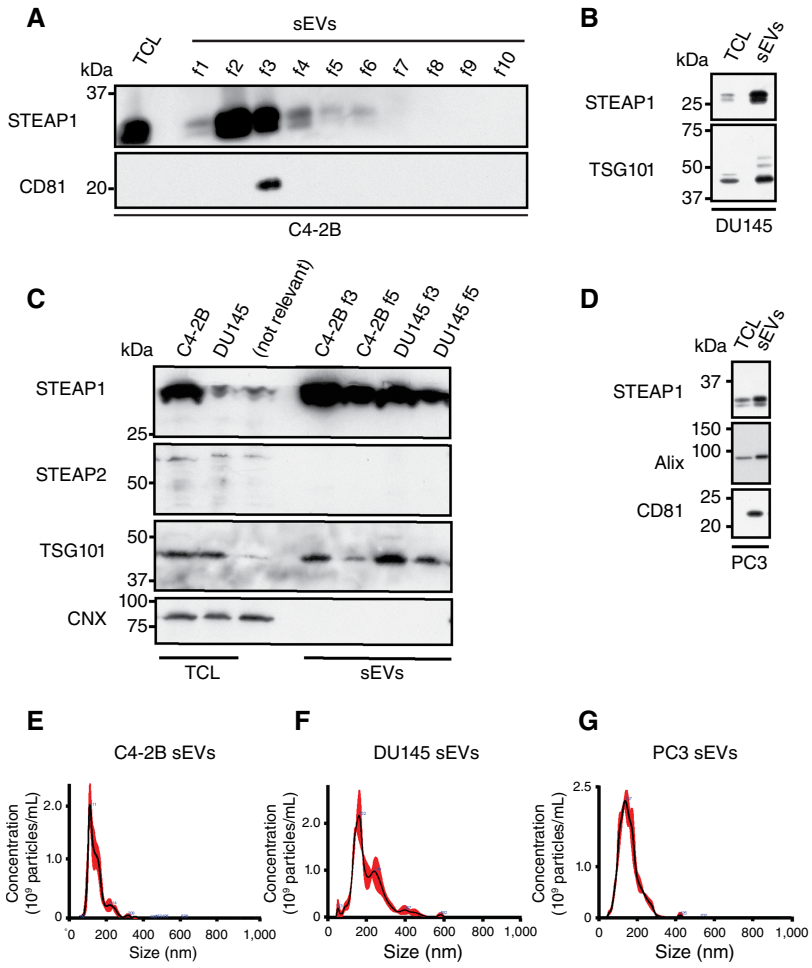


Figure 4.

STEAP1 is expressed in human prostate cancer cells and their derived sEVs. **A,** IB analysis of STEAP1 and CD81 in C4-2B total cell lysate (TCL) and lysates of sEV isolated by an IDG; 40 μg of C4-2B TCL and 10 μL out of 30 μL of each fraction were used. **B,** IB analysis of STEAP1 and TSG101 expression in DU145 cells and their derived sEVs; 37.5 μg of TCL and 10 μg of sEVs were used. **C,** IB analysis of STEAP1, STEAP2, TSG101, and CNX expression in C4-2B and DU145 cell lysates and their derived sEVs in fractions obtained by an IDG (f3) and 5 (f5); 40 μg of TCL and 6 μg of sEVs were used. **D,** IB analysis of STEAP1, Alix, and CD81 expression in PC3 cells and their derived sEVs; 20 μg of TCL and 4 μg of sEVs were used. **E–G,** NTA measurement of size distribution and concentration of IDG-isolated sEVs derived from (**E**) C4-2B, (**F**) DU145, and (**G**) PC3 cells.

within the prostate epithelium, resulting in reduced tumorigenicity potential (Supplementary Table S1).

sEVs from mouse plasma were isolated using IDG separation, and the obtained fractions were then combined into three sets based on their densities: ld-sEVs (1.099–1.130 g/mL), md-sEVs (1.148–1.186 g/mL), and hd-sEVs (1.189–1.195 g/mL). The ld-sEV derived from mouse plasma was excluded from the analysis because of the lack of STEAP1 expression in human prostate cancer–derived ld-sEVs. We assessed the expression of classical sEV markers Alix, CD9, and CD81 in the sEVs derived from the different mouse genotypes via IB analysis (**Fig. 5A–E**). Our results show that Alix and CD9 are expressed in md- and hd-sEVs derived from β1 FF, β1 FF TR, β1 FF Cre, and β1 FF Cre TR mouse plasma (**Fig. 5A–D**). When tested, CNX is absent from mouse plasma–derived sEVs. The sEV marker CD81 and the tyrosine kinase c-Src, previously shown by our group to be abundant in sEVs derived from mouse plasma (24), are also expressed in the β1 FF Cre TR–derived md- and hd-sEVs (**Fig. 5E**). Hence, regardless of β1 expression in the prostatic epithelium, all sEVs analyzed express comparable amounts of classical markers (**Fig. 5A–E**).

Furthermore, we assessed the expression of STEAP1 in sEVs derived from β1 FF, β1 FF TR, and β1 FF Cre TR mouse plasma (**Fig. 6**). IB analysis shows STEAP1 expression on all sEVs analyzed, irrespective of β1 expression (**Fig. 6A**). STEAP1 expression in md-sEVs from the normal genotype β1 FF and the cancer genotype β1 FF TR is comparable, and the levels observed are not significantly different (**Fig. 6B**; Supplementary Table S5). We analyzed the size distribution of sEVs derived from β1 FF or β1 FF TR (**Fig. 6C** and **D**) mouse plasma, as well as from wild-type and TR (Supplementary Fig. S5) mouse plasma as controls, using ZetaView. The analysis shows that the size of sEVs from all the genotypes analyzed is between 150–250 nm. We further confirm the size of sEVs from β1 FF and β1 FF TR using NTA (Supplementary Fig. S6). Our results show that regardless of β1 expression in the prostatic epithelium, all sEVs analyzed express comparable amounts of STEAP1. A summary of our findings can be found in **Fig. 7**.

Discussion

Our data show that a reduction of AR activity yields elevated *STEAP1* transcript and protein levels. The opposing expression profiles of STEAP1 and KLK3, along with the context-dependent influence of ARV7 status, suggest that AR-independent mechanisms influence STEAP1 expression in advanced disease. In the absence of androgen, we also show that STEAP1 and STEAP2, implicated in the exocytic pathway, are found in sEVs released from hormone-refractory prostate cancer cells and in circulating sEVs. This indicates that transcriptionally active AR is not required for packing STEAP1 into sEVs.

Downloaded from http://aacrjournals.org/mcr/article-pdf/doi/10.1158/1541-7786.MCR-24-0903/3597404/mcr-24-0903.pdf by Drexel University user on 19 May 2025

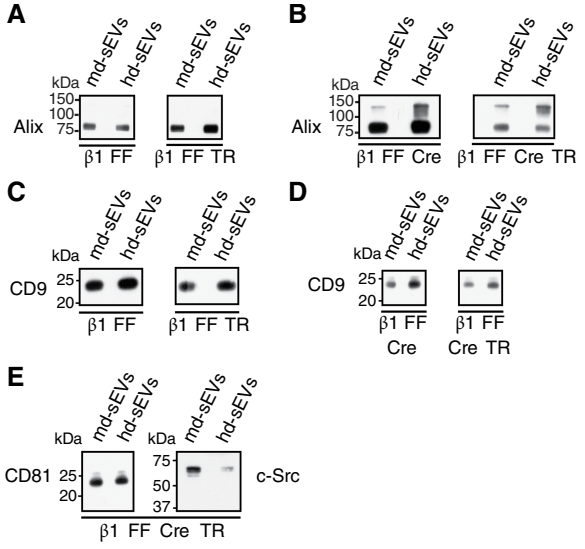


Figure 5.

Characterization of sEV markers in mouse plasma–derived sEVs. The collected sEV fractions derived from mouse plasma were pooled: md-sEVs are the middle-density fractions enriched in sEVs (md-sEVs), and hd-sEVs are the high-density fractions (hd-sEVs). IB analysis of Alix expression in IDG-isolated md- and hd-sEVs from (**A**) β1 FF and β1 FF TR (these lanes were spliced out of one single gel) and (**B**) β1 FF Cre and β1 FF Cre TR (these lanes were spliced out of one single gel); 4 and 7 μg of md- and hd-sEVs were used in **A** and **B**, respectively. IB analysis of CD9 expression in md- and hd-sEVs from (**C**) β1 FF and β1 FF TR (these lanes were spliced out of one single gel; 6 μg of md- and hd-sEVs were used) and (**D**) β1 FF Cre and β1 FF Cre TR (these lanes were spliced out of one single gel; 7 μg of md- and hd-sEVs were used). **E,** IB analysis of CD81 (left) and c-Src (right) expression in md- and hd-sEVs from β1 FF Cre TR mouse plasma; 6 μg of md- and hd-sEVs were used.

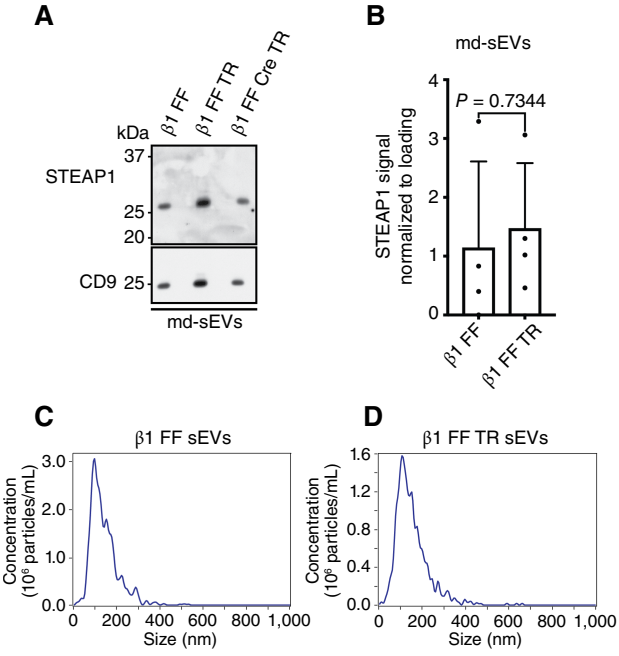


Figure 6.

STEAP1 characterization of sEVs derived from mouse plasma. **A,** IB analysis of STEAP1 and CD9 expression in IDG-isolated md-sEVs from β1 FF, β1 FF TR, and β1 FF Cre TR mouse plasma; 4 μg of sEVs were used. **B,** STEAP1 expression quantification normalized to loading control CD9. Four EV preparations per genotype were analyzed. The values are presented as individual replicates with error bars representing mean ± SEM. The *P* value was calculated using the Student *t* test. **C** and **D,** ZetaView NTA measurement of size distribution and concentration of IDG-isolated md-sEVs derived from (**C**) β1 FF or (**D**) β1 FF TR mouse plasma.

Gomes and colleagues (41) demonstrated that *STEAP1* is upregulated in response to androgen deprivation in HTS cells, as well as *in vivo* upon castration. Here, we show that the regulation of STEAP1 and STEAP2 under androgen deprivation remains consistent regardless of intrinsic hormone sensitivity and that alterations in AR status result in context-dependent expression patterns of both genes. Rocha and colleagues (42) reported that under full-hormone conditions, treatment with enzalutamide increases *STEAP1* transcript levels in HTS context. Similarly, we conclude that androgen depletion elicits context-dependent alterations in STEAP expression, though our data suggest that direct receptor antagonism does not have a substantial impact. This raises questions about the contribution of AR transcriptional activity versus its ligand, androgen, to the regulation of STEAP expression within distinct contexts. Future investigations should include the use of inhibitors targeting androgen stability and biosynthesis to determine if STEAP1 expression can be further altered.

Further complicating the picture of AR signaling in prostate cancer, single-cell RNA-seq revealed significant heterogeneity in gene regulatory networks associated with mCRPC and NEPC (6). This heterogeneity reflects substantial inter- and intrapatient variability, underscoring why treatment responses differ even among patients within the same clinical group. Investigations into NEPC revealed that deletion of *ACSL1* resulted in upregulation of *STEAP1* expression, indicating that restoration of STEAP expression can occur independently of AR (6, 43). *ACSL1* expression promotes a reversion to more luminal subtypes, suggesting that high *STEAP1* expression could represent a transitional state in which cells are no longer fully dependent on AR but have not yet acquired all NEPC characteristics.

The interplay between AR signaling and STEAP1 expression has significant implications for optimizing therapeutic strategies and drug development efforts at various stages of prostate cancer. The first-in-human clinical trial of xaluritamig (AMG 509), a STEAP1-directed bispecific T-cell engager, for advanced prostate cancer, showed encouraging clinical activity in heavily pretreated patients with mCRPC (18). Similarly, STEAP1-directed CAR-T cells displayed significant antitumor activity in a preclinical study and are currently in phase I/II clinical trials in combination with enzalutamide for men with mCRPC (NCT06236139; refs. 5, 17). Studies have shown that tumor cells will downregulate cell surface antigens to evade immune recognition through mechanisms of antigen escape (5, 44). *In vivo* evaluation of STEAP1 CAR-T cells indicated that prolonged exposure could result in loss of STEAP1 surface expression, suggesting a potential resistance mechanism (5, 44). The efficiency of immunotherapy is heavily dependent on antigen presentation and specificity (44). *In vitro* investigations revealed that AMG 509 preferentially targets cells with a high STEAP1 surface enrichment (45). Our findings show that androgen deprivation increases STEAP1 protein expression. This suggests that STEAP1-targeted therapies may be more effective in combination with ADT in early disease stages that are more reliant on AR signaling.

Downloaded from http://aacrjournals.org/mcr/article-pdf/doi/10.1158/1541-7786.MCR-24-0903/3597404/mcr-24-0903.pdf by Drexel University user on 19 May 2025

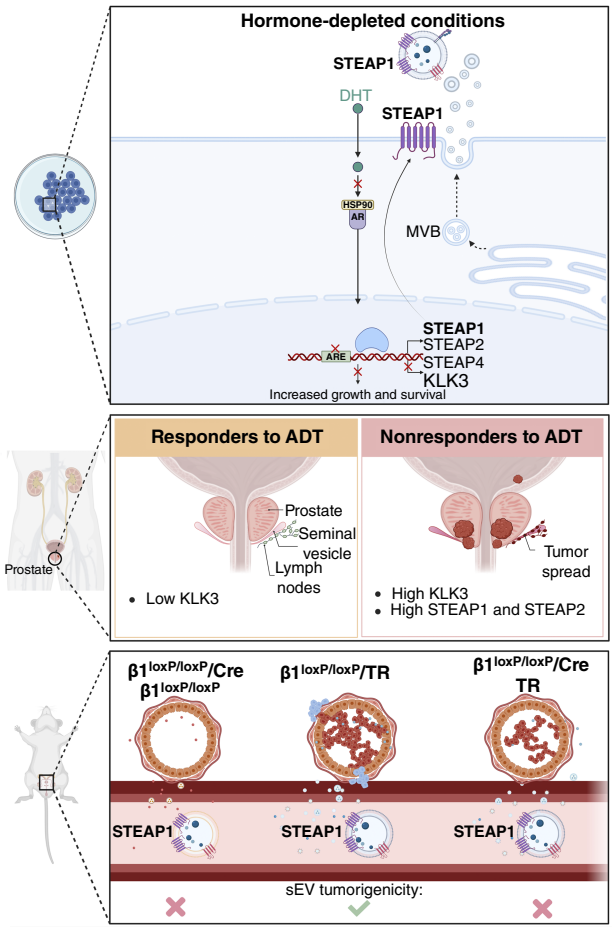


Figure 7.

Schematic drawing of the proposed model. Differential expression of the STEAP family members (STEAP1, STEAP2, and STEAP4) in prostate cancer cell lines in response to AR inhibition is shown in the top panel. Under androgen deprivation conditions, *STEAP1* and *STEAP2* exhibit elevated transcript levels, whereas *STEAP4* and *KLK3* expression is reduced. These results suggest differential AR regulation of the STEAP family in prostate cancer. STEAP1, but not STEAP2, is upregulated in sEVs from AR-negative (DU145 and PC3) and AR-positive (C4-2B) cells, indicating selective packaging of STEAP1 into sEVs independent of AR levels. Analysis of clinical data from patients with mCRPC reveals a strong positive correlation between AR activity and STEAP1/STEAP2 expression (middle panel). RNA-seq data from 210 mCRPC biopsies demonstrate patients with high AR activity (nonresponders) exhibit enriched STEAP1/STEAP2 expression, whereas responders to ADT show more variable STEAP1/STEAP2 levels as described in **Fig. 3C**. Finally, *ex vivo* analysis of circulating sEVs from genetically engineered mice with prostate cancer shows that STEAP1 is present in the sEV cargo, independent of β1 integrin expression in the prostatic epithelium (bottom panel). (Created with BioRender.com.)

However, further investigations are needed to confirm if all STEAP1 protein is trafficked to the cell membrane and whether its expression is sustained.

The expression of STEAP1 in sEVs, that we demonstrate here, has several therapeutic and diagnostic implications. High levels of STEAP1 and PSMA EVs have been detected and inversely correlated with tumor-reactive CD8 T-cell populations, indicating that EVs contribute to systemic immunosuppression in patients with mCRPC (46). Moreover, STEAP1 in sEVs has the potential to reduce the amount of available therapeutic drugs via off-tumor binding. This could potentially trigger misguided immune responses and contribute to the induction of CAR T-cell exhaustion effects by promoting hyper T-cell activation before reaching the tumor site (47).

We assessed STEAP1 and STEAP2 expression in human prostate cancer cells and their derived sEVs. We show a considerable increase in STEAP1 expression in sEVs derived from all models regardless of AR status. It has been observed that there is minimal STEAP1 expression in AR-negative cell lines (DU145 and PC3) compared with AR-positive (C4-2B) cells (48). The substantial increase in STEAP1 expression in DU145-derived sEVs suggests that the presence of STEAP1 in EVs is independent of its expression levels within the cell. Mariscal and colleagues (49) profiled the palmitoyl-proteome of large EVs and sEVs and found both STEAP1 and STEAP2 in sEVs from prostate cancer cells. This study showed a correlation between STEAP1 and prostate cancer but did not provide clinical data. In contrast with Mariscal and colleagues (49), we do not observe STEAP2 in DU145 cell–derived sEVs, which may be due to differences in detection methods, culture conditions, or that DU145 cells used in that study were genetically modified (49). The posttranslational modifications proposed by Gomes and colleagues (50) on STEAP1, including alterations in the glycosylation profile such as addition of O-linked β-N-acetylglucosamine, may contribute to differences in vesicle packaging between STEAP1 and STEAP2. Further studies are warranted to investigate alterations in the glycosylation profiles of STEAP1 in HTS and CRPC cells and their derived sEVs.

Our findings also show that STEAP1 is expressed in plasma sEVs derived from TR mice carrying prostate cancer, as well as from mice that do not carry tumors. The lack of significant differences between sEV samples from mice carrying prostate cancer compared with mice that do not have tumors may reflect limited aggressiveness of the disease model (24). These findings align with the current literature, which reports that STEAP1 has been identified in EVs derived from the plasma of patients with prostate cancer and healthy donors (49, 51). However, results from Lucien and colleagues (46) show that STEAP1 is strongly associated with metastasis and suggest that future studies should incorporate more aggressive prostate cancer models to better evaluate STEAP1 loading into EVs. In addition, we show that sEVs derived from the plasma of TR mice, which lack β1 integrin expression in the prostatic epithelium, carry STEAP1. As we had previously demonstrated that tumorigenicity of sEVs derived from TR mice depends on β1 integrin expression, we conclude that the loading or expression of STEAP1 in all the analyzed sEVs is independent of β1 integrins and may act via an unidentified pathway (24).

Androgen signaling modulates EV biogenesis influencing EV size, abundance, cargo composition, and selective packaging (51–53). *In vitro* DHT-stimulated AR activation promotes increased EV size, morphologic changes, and heterogeneous AR-driven cargo (52, 53). Conversely, androgen suppression enhances EV biogenesis, likely because of stress-related compensatory mechanisms, producing sEVs enriched in AR-independent survival factors and stress-related proteins (49, 52, 53). Clinically advanced disease correlates with elevated EV production driven by either overactive AR or adaptive resistance mechanisms arising from selective pressure of androgen blockade in heavily pretreated patients (46, 51). However, additional research is required to assess the impact of AR manipulation on STEAP1 expression in sEVs and the subsequent clinical implications.

Downloaded from http://aacrjournals.org/mcr/article-pdf/doi/10.1158/1541-7786.MCR-24-0903/3597404/mcr-24-0903.pdf by Drexel University user on 19 May 2025

Both clinical and *in vitro* data support the possibility that STEAP1 regulation involves a combination of androgen-dependent and -independent mechanisms (46, 49, 51–53). However, limited literature exists on the selective packaging and cargo loading of STEAP proteins, making this an active area of research. These findings underscore the complexity of tumor adaptation during disease progression, driven by the cellular microenvironment and stress conditions, resulting in significant molecular heterogeneity and variability in patient responses.

The parallel response observed for *STEAP1* and *STEAP2* under low-androgen conditions coupled with the detection of these molecules in sEVs across multiple disease stages illuminates the complexity surrounding AR signaling and STEAP regulation in prostate cancer. Notably, the detection of STEAP1 in EVs derived from AR-negative cell lines suggests potential AR-independent mechanisms driving its expression or loading in sEVs. Clinically, the detection of STEAP1 in EVs holds promise as a noninvasive method for real-time monitoring of therapeutic response. As STEAP-directed therapeutics continue to advance, a deeper understanding of the mechanisms that enhance STEAP1 expression will be critical to optimize therapeutic efficiency and identify the most appropriate stages in the disease continuum for administering STEAP1-targeted treatments.

Authors' Disclosures

W.K. Kelly reports being the principal investigator of a phase I study, as well as on a steering committee for the development of AMG 509, which is a T-cell engager to STEAP 1 (not received any personal compensation for any of these activities). M.J. Schiewer reports employment with Myriad Genetics starting April 16, 2024, which has had no influence on this work. No disclosures were reported by the other authors.

Authors' Contributions

C.L. Bizzaro: Conceptualization, data curation, formal analysis, funding acquisition, validation, investigation, visualization, methodology, writing–original draft, writing–review and editing. **C.A. Bach:** Conceptualization, formal analysis, funding acquisition, validation, investigation, visualization, methodology, writing–original draft, writing–review and editing. **R.A. Santos:** Conceptualization, formal analysis, validation, investigation, visualization, writing–review and editing. **C.E. Verrillo:** Validation, investigation, visualization, writing–review and editing. **N.M. Naranjo:** Validation, writing–review and editing. **I. Chaudhari:** Validation, investigation. **F.J. Picone:** Validation, investigation. **W. Iqbal:** Data curation, software, visualization, methodology, writing–review and editing. **A.G. Blidner:** Conceptualization, supervision, validation, writing–review and editing. **G.A. Rabinovich:** Conceptualization, supervision, validation, writing–review and editing. **A. Fatatis:** Conceptualization, resources, supervision, validation, writing–review and editing. **J. Jacobi:** Data curation, writing–review and editing. **D.W. Goodrich:** Conceptualization, resources, supervision, validation, writing–review and editing. **K.K. Zarrabi:** Conceptualization, supervision, validation, writing–review and editing. **W.K. Kelly:** Conceptualization, resources, supervision, funding acquisition, validation, project administration, writing–review and editing. **M.J. Schiewer:** Conceptualization, resources, supervision, validation, project administration, writing–review and editing. **L.R. Languino:** Conceptualization, resources, supervision, funding acquisition, validation, investigation, methodology, project administration, writing–review and editing.

Acknowledgments

The authors thank Dr. Lenny Gomella, Chair of the Urology Department at Thomas Jefferson University, for his support and guidance. The data acquisition, analysis, and project development for this manuscript would not have been possible without the guidance and feedback from Moriah Cunningham, PhD candidate; Latese Evans, MS; Salome Tchotorlishvili, MS; and Jasibel Vasquez-Gonzalez, all of whom are previous members of the Schiewer lab at Thomas Jefferson University. The authors would also like to thank the STEAP1 working group at Thomas Jefferson University for constructive criticism and project guidance. Dr. Md. Niamat Hossain, in Languino's laboratory, contributed to reviewing all the data and provided comments and corrections to the final manuscript version. This study was supported by R01 CA224769 and DoD W81XWH2210826 (to L.R. Languino); Philadelphia Prostate Cancer Biome Project (to L.R. Languino and C.L. Bizzaro); NIH/NCI R01CA217329 and R01CA255792 (to W.K. Kelly); P30CA056036 (to W.K. Kelly and A. Fatatis); and R01CA259358 (to A. Fatatis); PCF22CHAL13 and R01CA234162 (to D.W. Goodrich).

Note

Supplementary data for this article are available at Molecular Cancer Research Online (http://mcr.aacrjournals.org/).

Received October 22, 2024; revised December 24, 2024; accepted February 13, 2025; posted first April 27, 2025.

References

1. Siegel RL, Giaquinto AN, Jemal A. Cancer statistics, 2024. CA Cancer J Clin 2024;74:12–49.
2. Schiewer MJ, Knudsen KE. Basic science and molecular genetics of prostate cancer aggressiveness. Urol Clin North Am 2021;48:339–47.
3. Culig Z. Molecular mechanisms of enzalutamide resistance in prostate cancer. Curr Mol Biol Rep 2017;3:230–5.
4. Basil P, Robertson MJ, Bingman WE III, Dash AK, Krause WC, Shafi AA, et al. Cistrome and transcriptome analysis identifies unique androgen receptor (AR) and AR-V7 splice variant chromatin binding and transcriptional activities. Sci Rep 2022;12:5351.
5. Bhatia V, Kamat NV, Pariva TE, Wu LT, Tsao A, Sasaki K, et al. Targeting advanced prostate cancer with STEAP1 chimeric antigen receptor T cell and tumor-localized IL-12 immunotherapy. Nat Commun 2023;14:2041.
6. Zaidi S, Park J, Chan JM, Roudier MP, Zhao JL, Gopalan A, et al. Single-cell analysis of treatment-resistant prostate cancer: implications of cell state changes for cell surface antigen-targeted therapies. Proc Natl Acad Sci U S A 2024;121:e2322203121.
7. Xu M, Evans L, Bizzaro CL, Quaglia F, Verrillo CE, Li L, et al. STEAP1-4 (six-transmembrane epithelial antigen of the prostate 1–4) and their clinical implications for prostate cancer. Cancers (Basel) 2022;14:4034.
8. Grunewald TG, Bach H, Cossarizza A, Matsumoto I. The STEAP protein family: versatile oxidoreductases and targets for cancer immunotherapy with overlapping and distinct cellular functions. Biol Cell 2012;104:641–57.
9. Zhang Z, Hou WB, Zhang C, Tan YE, Zhang DD, An W, et al. A research of STEAP1 regulated gastric cancer cell proliferation, migration and invasion in vitro and in vivos. J Cell Mol Med 2020;24:14217–30.
10. Iijima K, Nakamura H, Takada K, Hayasaka N, Kubo T, Umeyama Y, et al. Six-transmembrane epithelial antigen of the prostate 1 accelerates cell proliferation by targeting c-Myc in liver cancer cells. Oncol Lett 2021;22:546.
11. Rocha SM, Santos FM, Socorro S, Passarinha LA, Maia CJ. Proteomic analysis of STEAP1 knockdown in human LNCaP prostate cancer cells. Biochim Biophys Acta Mol Cell Res 2023;1870:119522.
12. Chen WJ, Wu HT, Li CL, Lin YK, Fang ZX, Lin WT, et al. Regulatory roles of six-transmembrane epithelial antigen of the prostate family members in the occurrence and development of malignant tumors. Front Cell Dev Biol 2021;9:752426.
13. Gomes IM, Arinto P, Lopes C, Santos CR, Maia CJ. STEAP1 is overexpressed in prostate cancer and prostatic intraepithelial neoplasia lesions, and it is positively associated with Gleason score. Urol Oncol 2014;32:53.e23–9.
14. Challita-Eid PM, Morrison K, Etessami S, An Z, Morrison KJ, Perez-Villar JJ, et al. Monoclonal antibodies to six-transmembrane epithelial antigen of the prostate-1 inhibit intercellular communication in vitro and growth of human tumor xenografts in vivo. Cancer Res 2007;67:5798–805.
15. Yamamoto T, Tamura Y, Kobayashi JI, Kamiguchi K, Hirohashi Y, Miyazaki A, et al. Six-transmembrane epithelial antigen of the prostate-1 plays a role for

Downloaded from http://aacrjournals.org/mcr/article-pdf/doi/10.1158/1541-7786.MCR-24-0903/3597404/mcr-24-0903.pdf by Drexel University user on 19 May 2025

in vivo tumor growth via intercellular communication. Exp Cell Res 2013;319:2617–26.
16. Esmaeili SA, Nejatollahi F, Sahebkar A. Inhibition of intercellular communication between prostate cancer cells by A specific anti-STEAP-1 single chain antibody. Anticancer Agents Med Chem 2018;18:1674–9.
17. Jin Y, Lorvik KB, Jin Y, Beck C, Sike A, Persiconi I, et al. Development of STEAP1 targeting chimeric antigen receptor for adoptive cell therapy against cancer. Mol Ther Oncolytics 2022;26:189–206.
18. Kelly WK, Danila DC, Lin CC, Lee JL, Matsubara N, Ward PJ, et al. Xaluritamig, a STEAP1 × CD3 XmAb 2+1 immune therapy for metastatic castration-resistant prostate cancer: results from dose exploration in a first-in-human study. Cancer Discov 2024;14:76–89.
19. Zanvit P, van Dyk D, Fazenbaker C, McGlinchey K, Luo W, Pezold JM, et al. Antitumor activity of AZD0754, a dnTGFβRII-armored, STEAP2-targeted CAR-T cell therapy, in prostate cancer. J Clin Invest 2023;133:e169655.
20. Kalluri R, LeBleu VS. The biology, function, and biomedical applications of exosomes. Science 2020;367:eaau6977.
21. Mathieu M, Martin-Jaular L, Lavieu G, Théry C. Specificities of secretion and uptake of exosomes and other extracellular vesicles for cell-to-cell communication. Nat Cell Biol 2019;21:9–17.
22. Möller A, Lobb RJ. The evolving translational potential of small extracellular vesicles in cancer. Nat Rev Cancer 2020;20:697–709.
23. Wortzel I, Dror S, Kenific CM, Lyden D. Exosome-mediated metastasis: communication from a distance. Dev Cell 2019;49:347–60.
24. DeRita RM, Sayeed A, Garcia V, Krishn SR, Shields CD, Sarker S, et al. Tumor-derived extracellular vesicles require β1 integrins to promote anchorage-independent growth. iScience 2019;14:199–209.
25. Quaglia F, Krishn SR, Daaboul GG, Sarker S, Pippa R, Domingo-Domenech J, et al. Small extracellular vesicles modulated by αVβ3 integrin induce neuroendocrine differentiation in recipient cancer cells. J Extracell Vesicles 2020;9:1761072.
26. Krishn SR, Salem I, Quaglia F, Naranjo NM, Agarwal E, Liu Q, et al. The αvβ6 integrin in cancer cell-derived small extracellular vesicles enhances angiogenesis. J Extracell Vesicles 2020;9:1763594.
27. Hoshino A, Costa-Silva B, Shen TL, Rodrigues G, Hashimoto A, Tesic Mark M, et al. Tumour exosome integrins determine organotropic metastasis. Nature 2015;527:329–35.
28. Singh A, Fedele C, Lu H, Nevalainen MT, Keen JH, Languino LR. Exosome-mediated transfer of αvβ3 integrin from tumorigenic to nontumorigenic cells promotes a migratory phenotype. Mol Cancer Res 2016;14:1136–46.
29. Goel HL, Sayeed A, Breen M, Zarif MJ, Garlick DS, Leav I, et al. β1 integrins mediate resistance to ionizing radiation in vivo by inhibiting c-Jun amino terminal kinase 1. J Cell Physiol 2013;228:1601–9.
30. Schiewer MJ, Goodwin JF, Han S, Brenner JC, Augello MA, Dean JL, et al. Dual roles of PARP-1 promote cancer growth and progression. Cancer Discov 2012;2:1134–49.
31. Naranjo NM, Salem I, Harris MA, Languino LR. IFIT3 (interferon induced protein with tetratricopeptide repeats 3) modulates STAT1 expression in small extracellular vesicles. Biochem J 2021;478:3905–21.
32. Salem I, Naranjo NM, Singh A, DeRita R, Krishn SR, Sirman LS, et al. Methods for extracellular vesicle isolation from cancer cells. Cancer Drug Resist 2020;3:1–14.
33. Quaglia F, Krishn SR, Wang Y, Goodrich DW, McCue P, Kossenkov AV, et al. Differential expression of αVβ3 and αVβ6 integrins in prostate cancer progression. PLoS One 2021;16:e0244985.
34. Abida W, Cyrta J, Heller G, Prandi D, Armenia J, Coleman I, et al. Genomic correlates of clinical outcome in advanced prostate cancer. Proc Natl Acad Sci U S A 2019;116:11428–36.
35. Cerami E, Gao J, Dogrusoz U, Gross BE, Sumer SO, Aksoy BA, et al. The cBio cancer genomics portal: an open platform for exploring multidimensional cancer genomics data. Cancer Discov 2012;2:401–4.
36. Gao J, Aksoy BA, Dogrusoz U, Dresdner G, Gross B, Sumer SO, et al. Integrative analysis of complex cancer genomics and clinical profiles using the cBioPortal. Sci Signal 2013;6:pl1.
37. de Bruijn I, Kundra R, Mastrogiacomo B, Tran TN, Sikina L, Mazor T, et al. Analysis and visualization of longitudinal genomic and clinical data from the AACR project GENIE biopharma collaborative in cBioPortal. Cancer Res 2023;83:3861–7.
38. Lundberg A, Zhang M, Aggarwal R, Li H, Zhang L, Foye A, et al. The genomic and epigenomic landscape of double-negative metastatic prostate cancer. Cancer Res 2023;83:2763–74.
39. DiNatale A, Worrede A, Iqbal W, Marchioli M, Toth A, Sjöström M, et al. IL-1β expression driven by androgen receptor absence or inactivation promotes prostate cancer bone metastasis. Cancer Res Commun 2022;2:1545–57.
40. Quigley DA, Dang HX, Zhao SG, Lloyd P, Aggarwal R, Alumkal JJ, et al. Genomic hallmarks and structural variation in metastatic prostate cancer. Cell 2018;174:758–69.e9.
41. Gomes IM, Santos CR, Socorro S, Maia CJ. Six transmembrane epithelial antigen of the prostate 1 is down-regulated by sex hormones in prostate cells. Prostate 2013;73:605–13.
42. Rocha SM, Nascimento D, Cardoso AM, Passarinha L, Socorro S, Maia CJ. STEAP1 regulation and its influence modulating the response of LNCaP prostate cancer cells to bicalutamide, enzalutamide and apalutamide. Mol Med Rep 2023;27:52.
43. Ku SY, Wang Y, Garcia MM, Yamada Y, Mizuno K, Long MD, et al. Notch signaling suppresses neuroendocrine differentiation and alters the immune microenvironment in advanced prostate cancer. J Clin Invest 2024;134:e175217.
44. Angappulige DH, Mahajan NP, Mahajan K. Epigenetic underpinnings of tumor-immune dynamics in prostate cancer immune suppression. Trends Cancer 2024;10:369–81.
45. Nolan-Stevaux O, Li C, Liang L, Zhan J, Estrada J, Osgood T, et al. AMG 509 (Xaluritamig), an anti-STEAP1 XmAb 2+1 T-cell redirecting immune therapy with avidity-dependent activity against prostate cancer. Cancer Discov 2024;14:90–103.
46. Lucien F, Kim Y, Qian J, Orme JJ, Zhang H, Arafa A, et al. Tumor-derived extracellular vesicles predict clinical outcomes in oligometastatic prostate cancer and suppress antitumor immunity. Int J Radiat Oncol Biol Phys 2022;114:725–37.
47. Wang S, Sun J, Dastgheyb RM, Li Z. Tumor-derived extracellular vesicles modulate innate immune responses to affect tumor progression. Front Immunol 2022;13:1045624.
48. Hubert RS, Vivanco I, Chen E, Rastegar S, Leong K, Mitchell SC, et al. STEAP: a prostate-specific cell-surface antigen highly expressed in human prostate tumors. Proc Natl Acad Sci U S A 1999;96:14523–8.
49. Mariscal J, Vagner T, Kim M, Zhou B, Chin A, Zandian M, et al. Comprehensive palmitoyl-proteomic analysis identifies distinct protein signatures for large and small cancer-derived extracellular vesicles. J Extracell Vesicles 2020;9:1764192.
50. Gomes IM, Santos CR, Maia CJ. Expression of STEAP1 and STEAP1B in prostate cell lines, and the putative regulation of STEAP1 by post-transcriptional and post-translational mechanisms. Genes Cancer 2014;5:142–51.
51. Khanna K, Salmond N, Lynn KS, Leong HS, Williams KC. Clinical significance of STEAP1 extracellular vesicles in prostate cancer. Prostate Cancer Prostatic Dis 2021;24:802–11.
52. Soekmadji C, Riches JD, Russell PJ, Ruelcke JE, McPherson S, Wang C, et al. Modulation of paracrine signaling by CD9 positive small extracellular vesicles mediates cellular growth of androgen deprived prostate cancer. Oncotarget 2017;8:52237–55.
53. Martens-Uzunova ES, Kusuma GD, Crucitta S, Lim HK, Cooper C, Riches JE, et al. Androgens alter the heterogeneity of small extracellular vesicles and the small RNA cargo in prostate cancer. J Extracell Vesicles 2021;10:e12136.

Downloaded from http://aacrjournals.org/mcr/article-pdf/doi/10.1158/1541-7786.MCR-24-0903/3597404/mcr-24-0903.pdf by Drexel University user on 19 May 2025